

MHD flow and heat transfer of Sisko fluid over a radially stretching sheet with convective boundary conditions

Masood Khan¹ · Rabia Malik¹ · Asif Munir¹ · Azeem Shahzad²

Received: 9 December 2014 / Accepted: 16 September 2015 / Published online: 29 September 2015
© The Brazilian Society of Mechanical Sciences and Engineering 2015

Abstract This paper analyzes magnetohydrodynamic axisymmetric flow of an electrically conducting Sisko fluid over a radially stretching surface. The analysis includes forced convective heat transfer by considering convective boundary conditions. The transformed nonlinear governing ordinary differential equations are solved analytically as well as numerically by utilizing the homotopy analysis method (HAM) and shooting method, respectively. As a result of the analysis, some exact solutions for the velocity and temperature distributions are obtained and a comparison is made with the HAM solutions with an excellent agreement.

Keywords Axisymmetric flow · Convective heat transfer · Sisko fluid · Convective boundary conditions

1 Introduction

Rapid progress in various fields of science and technology has urged from researchers to extend their studies toward the regime of non-Newtonian fluids and their heat transfer characteristics. It is due to the fact that most non-Newtonian fluids have more profuse industrial and technological applications rather than Newtonian fluids. It is a wider class of fluids

which cannot be described by a single model. The capability of each model for depicting the fluid properties is restricted to a certain range. Among these models, a model describing one of the most commonly existing nature of fluid namely, shear thinning and shear thickening, is known as Sisko fluid model [1]. The flow of greases can be most appropriately described by aforementioned model [2]. Some of its industrial applications include cement slurries, drilling fluids, waterborne coatings, and most pseudoplastic fluids [3, 4].

In processes where high temperature is evoked, the convective heat transfer is of incredible importance, for instance, nuclear plants, gas turbines, and storage of thermal energy and so forth. To define the linear convective heat exchange condition for algebraic entities, the convective boundary conditions are considered. It is agreed that the convective boundary conditions are more practical in various industrial and engineering processes, for instance, transpiration cooling process, material drying, etc. The practical importance of the convective boundary conditions has compelled many researchers to investigate and report their findings on this topic. Hayat et al. [5] examined the heat transfer in an upper-convected Maxwell fluid over a moving surface along with the convective boundary conditions. Similarly, Makinde et al. [6] studied the unsteady flow of a pressure driven third-grade fluid through a porous saturated medium considering thermal effects, variable viscosity, and convective boundary conditions. Hayat et al. [7] studied flow and heat transfer of Eyring Powell fluid over a moving surface in the presence of convective boundary conditions. Likewise, Rundora and Makinde [8] discussed the influence of suction/injection on unsteady reactive temperature-dependent viscosity of third-grade fluid flow in a channel filled with porous medium taking into account the convective boundary conditions. They obtained the results using semi-implicit finite difference scheme. Ramesh and Gireesha [9] studied the effects of heat source/sink on the Maxwell fluid over a

Technical Editor: Roney Leon Thompson.

✉ Rabia Malik
rabiamalik.qau@gmail.com

¹ Department of Mathematics, Quaid-i-Azam University, Islamabad, Pakistan

² Department of Basic Science, University of Engineering & Technology, Taxila, Pakistan

stretching sheet with convective boundary condition, while nanoparticles are also taken into account. Shahzad et al. [10] obtained the series solution for the three-dimensional flow of Jeffrey fluid over a stretched surface with convective boundary condition. Nadeem et al. [11] examined the stagnation point flow of a Casson nanofluid with convective boundary conditions and the optimal homotopy analysis method is employed to solve analytically the resulting problem equations.

Recently the researchers and scientists are intrigued to reduce the skin-friction coefficient and enhance the rate of heating or cooling in the advanced technological processes. Therefore, various attempts have been made about the reduction of skin friction or drag forces for flows over the surface of a tail plane, wing, wind turbine rotor, and so forth. However, these forces can be reduced by keeping the boundary layer away from separation and delaying the transition of laminar to turbulent flow. This task can be performed through different physical aspects such as moving the surface, through fluid suction and injection and the presence of body forces. Similarly most of the researchers have been tried to enhance the rate of cooling/heating by using different types of boundary conditions over a flat plate. To overcome such difficulties, this paper aims at providing the analytical solutions for forced convective heat transfer of an electrically conducting Sisko fluid over a nonlinear radially stretching sheet, while taking the effects of convective boundary conditions into consideration. The solution of the governing problem is obtained analytically by using the homotopy analysis method and numerically by shooting technique.

2 Formulation of the problem

Consider the steady, two-dimensional (r, z) convective boundary layer flow of an electrically conducting Sisko fluid over a nonlinear radially stretching sheet placed at $z = 0$. The flow is induced by stretching of the sheet with velocity $U = cr^s$, where c and s are non-negative real numbers. A uniform magnetic field $\mathbf{B} = [0, B_0, 0]$ perpendicular to the plane of sheet is applied under the assumption of very small magnetic Reynolds number. It is assumed that the bottom surface of the sheet is heated by convection from a hot fluid at temperature T_f which provides a heat transfer coefficient h_f . Further, the ambient fluid temperature is T_∞ . The boundary layer governing equations for the steady conservation of mass, momentum, and thermal energy can be written as follows (see Ref. [4] for details):

$$\frac{\partial u}{\partial r} + \frac{u}{r} + \frac{\partial w}{\partial z} = 0, \tag{1}$$

$$u \frac{\partial u}{\partial r} + w \frac{\partial u}{\partial z} = \frac{a}{\rho} \frac{\partial^2 u}{\partial z^2} - \frac{b}{\rho} \frac{\partial}{\partial z} \left(-\frac{\partial u}{\partial z} \right)^n - \frac{\sigma B_0^2}{\rho} u, \tag{2}$$

$$u \frac{\partial T}{\partial r} + w \frac{\partial T}{\partial z} = \alpha \frac{\partial^2 T}{\partial z^2}, \tag{3}$$

where u and w are the components of velocity in the radial and axial directions, respectively, T the temperature field, a , b , and n (≥ 0) are the material constants, ρ the fluid density, σ the electrical conductivity of the fluid, B_0 the magnitude of applied magnetic field, $\alpha = \frac{k}{\rho c_p}$ the thermal diffusivity with c_p as the specific heat of fluid at constant pressure, and k the thermal conductivity.

Equations (1)–(3) are subjected to the following boundary conditions:

$$u(r, z) = U = cr^s, \quad w(r, z) = 0, \tag{4}$$

$$k \frac{\partial T(r, z)}{\partial z} = -h_f [T_f - T(r, z)] \quad \text{at } z = 0,$$

$$u \rightarrow 0, \quad T \rightarrow T_\infty \quad \text{as } z \rightarrow \infty. \tag{5}$$

The governing Eqs. (1)–(3) subject to the boundary conditions (4) and (5) can be expressed in simpler form by introducing the following suitable transforms:

$$\eta = \frac{z}{r} \text{Re}_b^{\frac{1}{n+1}}, \quad \psi = -Ur^2 \text{Re}_b^{-\frac{1}{n+1}} f(\eta), \tag{6}$$

where η is the independent variable and ψ the Stokes stream function.

By employing the transformations (6), the above governing problem reduces to the following:

$$Af''' + n(-f'')^{n-1} f''' + \frac{s(2n-1) + n + 2}{n+1} ff'' - s(f')^2 - M^2 f' = 0, \tag{7}$$

$$\theta'' + \frac{s(2n-1) + n + 2}{n+1} \text{Pr} f \theta' = 0, \tag{8}$$

$$f(0) = 0, \quad f'(0) = 1, \quad \theta'(0) = -\gamma [1 - \theta(0)], \tag{9}$$

$$f'(\eta) \rightarrow 0, \quad \theta(\eta) \rightarrow 0 \quad \text{as } \eta \rightarrow \infty. \tag{10}$$

In the above equations, primes denote differentiation with respect to η . Further, A is the material parameter of the Sisko fluid, M the magnetic parameter, Re_a and Re_b the local Reynolds numbers, Pr the generalized Prandtl number, and γ the generalized Biot number, which are defined as follows:

$$M^2 = \frac{\sigma B_0^2}{\rho U}, \quad \text{Re}_a = \frac{\rho r U}{a}, \quad \text{Re}_b = \frac{\rho r^n U^{2-n}}{b}, \quad A = \frac{\text{Re}_b^{\frac{2}{n+1}}}{\text{Re}_a},$$

$$\gamma = \frac{h_f}{k} r \text{Re}_b^{-\frac{1}{n+1}}, \quad \text{Pr} = \frac{r U}{\alpha} \text{Re}_b^{-\frac{2}{n+1}}. \tag{11}$$

The physical quantities of interest are the local skin-friction coefficient C_f and the local Nusselt number Nu which are defined by the following:

$$\frac{1}{2} \text{Re}_b^{\frac{1}{n+1}} C_f = Af''(0) - [-f''(0)]^n, \tag{12}$$

$$\text{Re}_b^{-\frac{1}{n+1}} Nu = -\theta'(0). \tag{13}$$

3 The exact solution

The set of Eqs. (7) and (8) subject to the boundary conditions (9) and (10) is highly nonlinear. In addition, the power-law index n is a non-negative real number and hence finding the exact solution of the system in general is a far from any routine exercise. However, exact solutions of the system are calculated for some special cases given below.

Case (i) For $n = 0$ and $s = 1$, Eqs. (7) and (8) reduce to

$$Af''' + ff'' - (f')^2 - M^2f' = 0, \tag{14}$$

$$\theta'' + \text{Pr}f\theta' = 0. \tag{15}$$

The exact solutions of Eqs. (14) and (15) satisfying the boundary conditions (9) and (10) are as follows:

$$f(\eta) = \frac{1}{\beta}(1 - e^{-\beta\eta}), \tag{16}$$

$$\theta(\eta) = \frac{e^{\frac{\text{Pr}}{\beta^2}\eta} \gamma \left[\Gamma\left(\frac{\text{Pr}}{\beta^2}, 0\right) - \Gamma\left(\frac{\text{Pr}}{\beta^2}, \frac{\text{Pr}}{\beta^2}e^{-\beta\eta}\right) \right]}{\beta \left(\frac{\text{Pr}}{\beta^2}\right)^{\frac{\text{Pr}}{\beta^2}} + e^{\frac{\text{Pr}}{\beta^2}\eta} \gamma \left[\Gamma\left(\frac{\text{Pr}}{\beta^2}, 0\right) - \Gamma\left(\frac{\text{Pr}}{\beta^2}, \frac{\text{Pr}}{\beta^2}\right) \right]}, \tag{17}$$

where $\beta = \sqrt{\frac{1+M^2}{A}}$ and $\Gamma(\cdot)$ the incomplete Gamma function.

Table 1 The convergence of the series solution when $s = M = A = \gamma = \text{Pr} = 1$ and $n = 2$ are fixed

Order of approximation	$-\frac{1}{2} \text{Re}_b^{\frac{1}{n+1}} C_f$	$-\text{Re}_b^{-\frac{1}{n+1}} Nu$
1	2.079804	0.480960
5	2.117063	0.489321
11	2.117186	0.489558
13	2.117188	0.489572
16	2.117189	0.489573
18	2.117189	0.489573
20	2.117189	0.489573
25	2.117189	0.489573

Case (ii) Next for $n = 1$ and $s = 3$, Eqs. (7) and (8) take the form

$$(1 + A)f''' + 3ff'' - 3(f')^2 - M^2f' = 0, \tag{18}$$

$$\theta'' + 3\text{Pr}f\theta' = 0. \tag{19}$$

The exact analytical solutions to Eqs. (18)–(19) together with the boundary conditions (9) and (10) are in the following form:

$$f(\eta) = \frac{1}{\beta}(1 - e^{-\beta\eta}), \tag{20}$$

$$\theta(\eta) = \frac{e^{\frac{3\text{Pr}}{\beta^2}\eta} \gamma \left[\Gamma\left(\frac{3\text{Pr}}{\beta^2}, 0\right) - \Gamma\left(\frac{3\text{Pr}}{\beta^2}, \frac{3\text{Pr}}{\beta^2}e^{-\beta\eta}\right) \right]}{\beta \left(\frac{3\text{Pr}}{\beta^2}\right)^{\frac{3\text{Pr}}{\beta^2}} + e^{\frac{3\text{Pr}}{\beta^2}\eta} \gamma \left[\Gamma\left(\frac{3\text{Pr}}{\beta^2}, 0\right) - \Gamma\left(\frac{3\text{Pr}}{\beta^2}, \frac{3\text{Pr}}{\beta^2}\right) \right]}, \tag{21}$$

with $\beta = \sqrt{\frac{3+M^2}{1+A}}$.

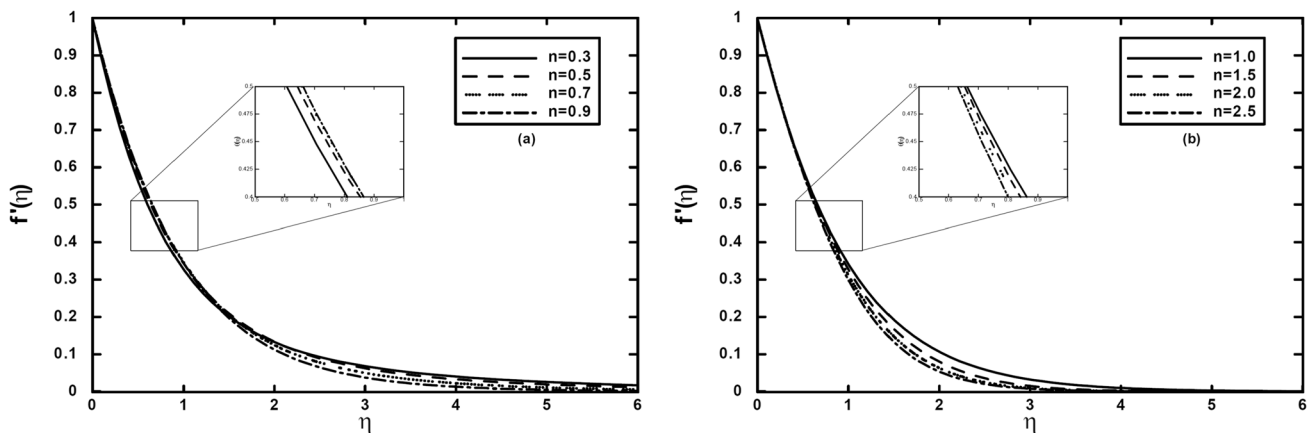


Fig. 1 The velocity profiles $f'(\eta)$ for different values of the power-law index n when $A = M = 1$ and $s = 1/2$ are fixed

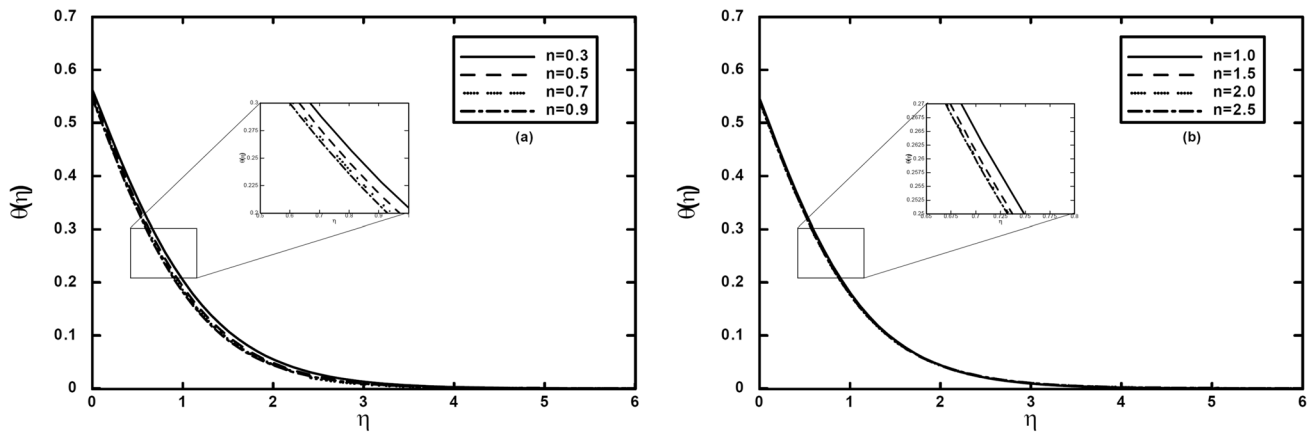


Fig. 2 The temperature profiles $\theta(\eta)$ for different values of the power-law index n when $M = Pr = A = \gamma = 1$ and $s = 1/2$ are fixed

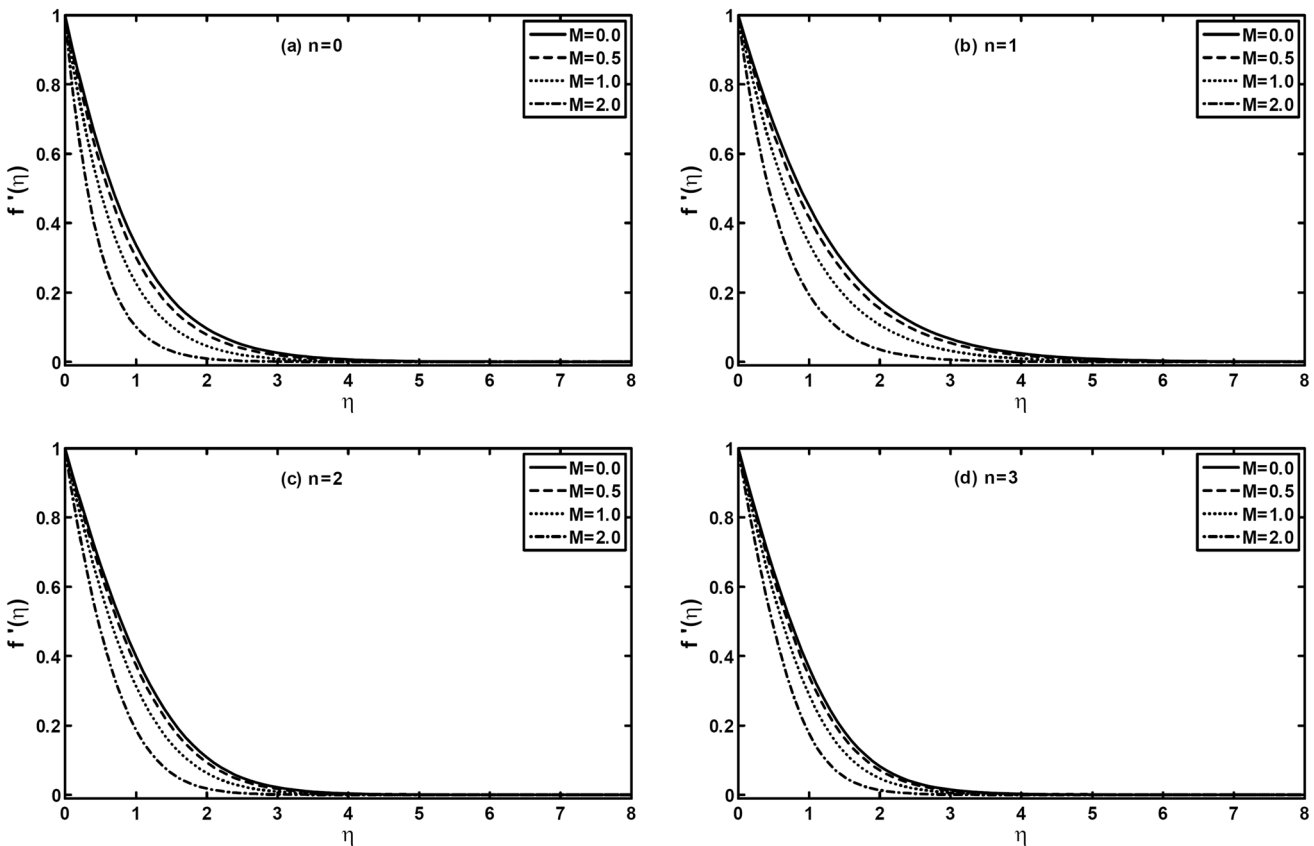


Fig. 3 The velocity profiles $f'(\eta)$ for different values of the magnetic parameter M when $A = 1$ and $s = 1/2$ are fixed

4 Solution methodologies

4.1 The HAM analytic solution

The analytic series solutions for the velocity and temperature fields are obtained for the nonlinear Eqs. (7) and (8)

together with the boundary conditions (9) and (10) by utilizing the homotopy analysis method [12–14]. The convergence of these series solutions is highly dependent upon the selection of the auxiliary parameter \hbar , which we have calculated by using the squared residual error which is defined by the following: [15]

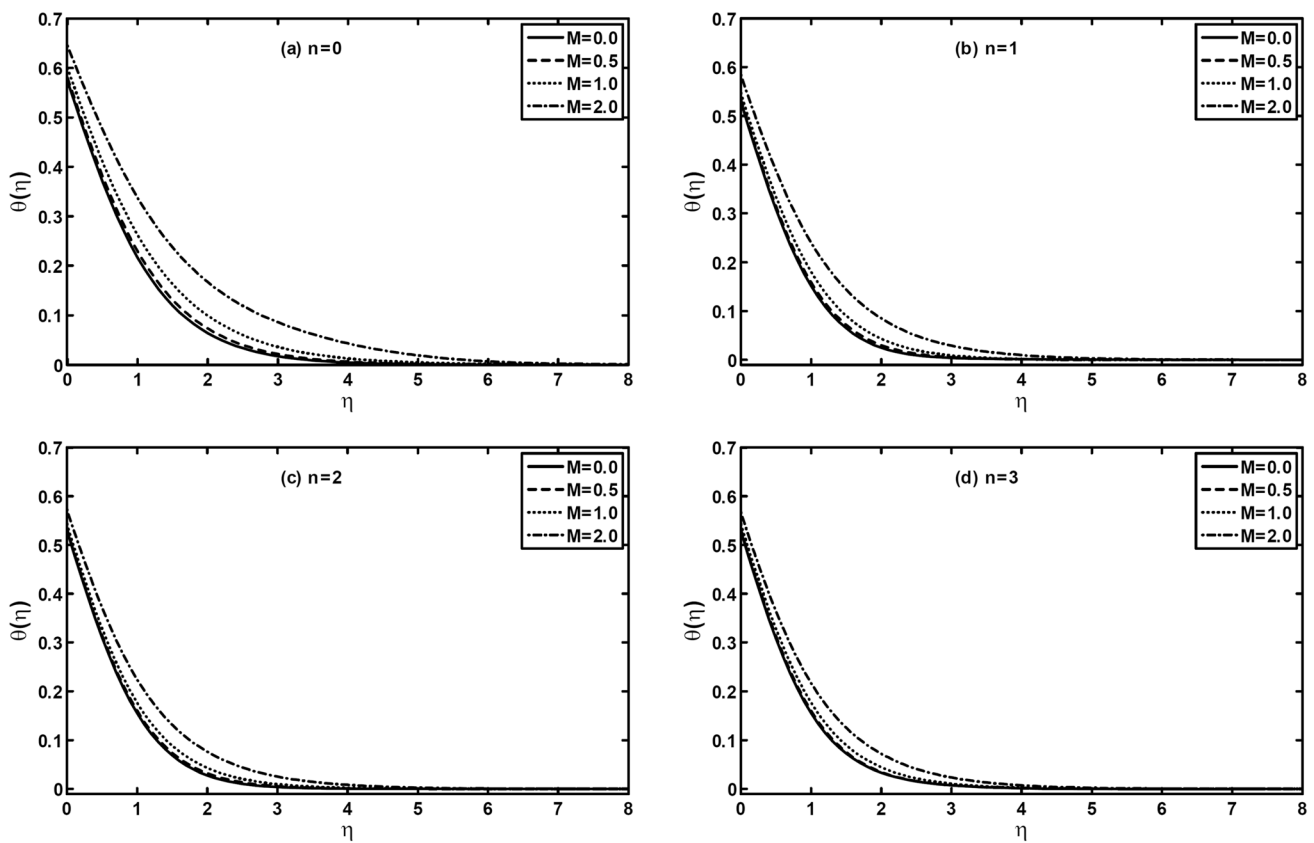


Fig. 4 The temperature profiles $\theta(\eta)$ for different values of the magnetic parameter M when $A = Pr = \gamma = 1$ and $s = 1/2$ are fixed

$$E_{f,m} = \frac{1}{N+1} \sum_{j=0}^N \left[N_f \left(\sum_{i=0}^m f_j(i\Delta\eta) \right) \right]^2. \tag{22}$$

Table 1 depicts the convergence of the series solution for a specific case. Considering the most suitable value of h , the convergence is achieved at sixteenth order of approximation.

4.2 The numerical solution

The nonlinear Eqs. (7) and (8) governing the problem along with the boundary conditions (9) and (10) form a set of boundary value problems (BVPs). These BVPs are first converted into a set of initial value problems (IVPs) and then solved numerically by utilizing the shooting method. We have converted Eqs. (7) and (8) into system of first order equations as follows:

$$f' = p, p' = q, q' = -\frac{1}{A + n(-q)^{n-1}} \left[\frac{s(2n-1) + n + 2}{n+1} fq - sp^2 - M^2p \right], \tag{23}$$

$$\theta' = g, g' = -\frac{s(2n-1) + n + 2}{n+1} Prfg, \tag{24}$$

with boundary conditions

$$f(0) = 0, p(0) = 1, g(0) = -\gamma[1 - \theta(0)]. \tag{25}$$

Now to solve Eqs. (23) and (24) as initial value problems, we need values for $f'(0)$ and $\theta'(0)$ which are not defined. So we choose values for $f''(0)$ and $\theta''(0)$ and obtain the solution by using fourth-order Runge–Kutta method. The obtained values of $f'(\eta)$ and $\theta(\eta)$ as $\eta \rightarrow \infty$ say η_∞ are compared with the given boundary conditions $f(\eta_\infty) = 0$ and $\theta(\eta_\infty) = 0$. Then to get better approximation for our solution, $f''(0)$ and $\theta''(0)$ are adjusted using secant method. Here we have considered step size $h = 0.01$. Until we approach the desired accuracy of our results, the process is repeated.

5 Results and discussion

The non-dimensional equations of convective MHD boundary layer flow of Sisko fluid over a radially stretching sheet are studied. The system of coupled ordinary

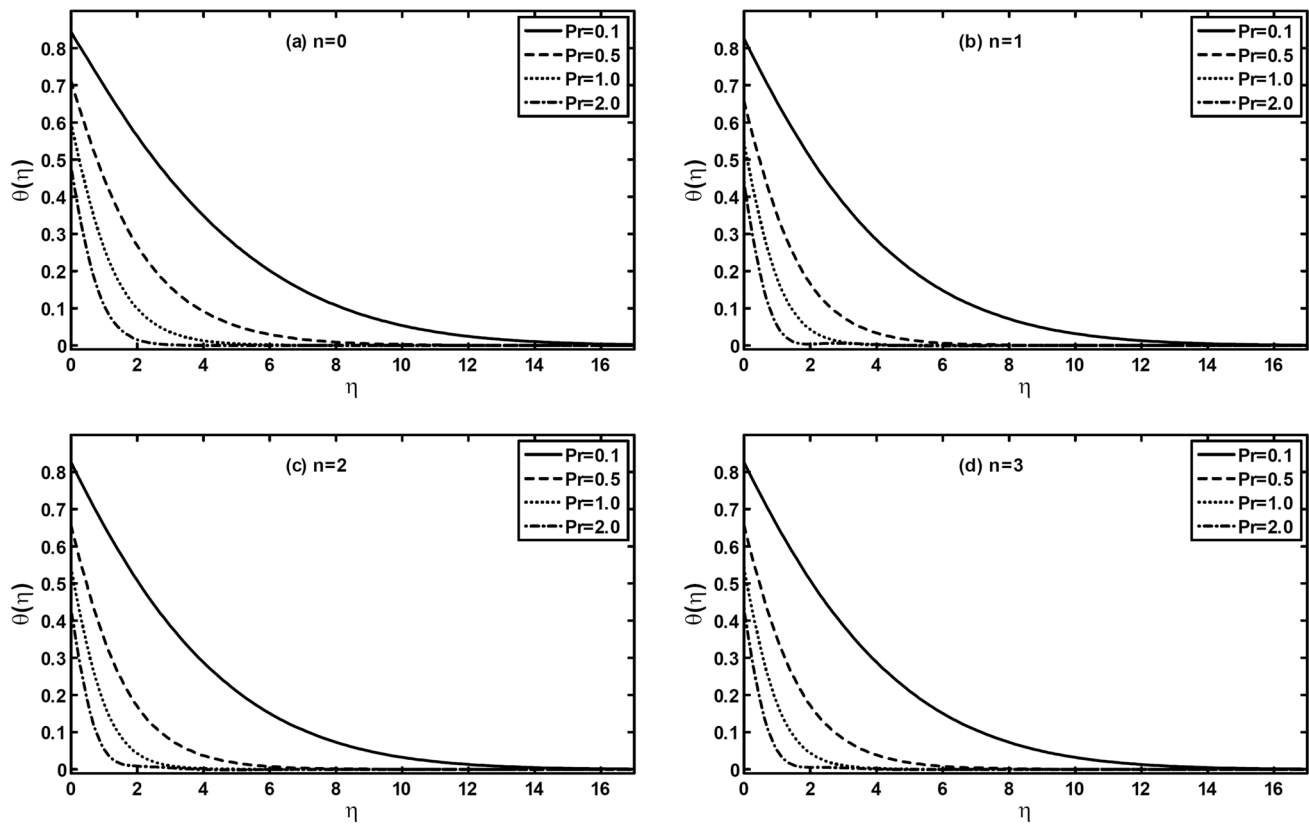


Fig. 5 The temperature profiles $\theta(\eta)$ for different values of the generalized Prandtl number Pr when $A = M = \gamma = 1$ and $s = 1/2$ are fixed

differential Eqs. (7) and (8) subject to convective boundary conditions (9) and (10) is solved analytically using the HAM and numerically using the shooting method. In addition, exact solutions for particular cases, where possible, are constructed. Further, the numerical values of the local skin-friction coefficient and local Nusselt number with varying physical parameters are recorded through tables. It is worth pointing out that the parameter which controls the power-law behavior of the fluid, called the power-law index n , appears in the equations and is a non-negative real number. The HAM results are only for integer values of the power-law index n , whereas the results for non-integer values of the power-law index n are obtained numerically.

Figures 1 and 2 show the influence of the power-law index n on the velocity and temperature profiles, respectively. It can be seen in these figures that inside the boundary layer the value of n effects significantly the velocity field but marginally the temperature field. It is observed from velocity profiles presented that for $n < 1$ (pseudo-plastic or shear thinning fluids), as n increases, the velocity profile increases near the surface but it decreases far away from the surface. For $n > 1$ (dilatant or shear thickening fluids), as n increases, the velocity profile decreases

throughout the domain. This results in a decrease in the boundary layer thickness for both shear thinning and shear thickening fluids. However, the apparent viscosity increases for $n < 1$ and decreases for $n > 1$ and as a consequence the viscous effects are transmitted up to a greater distance from the plate and the boundary layer thickness is thicker for $n < 1$ as compared to $n > 1$. From the temperature profile presented, it is noticed that for both $n < 1$ and $n > 1$, the temperature as well as thermal boundary layer thickness reduces with an increase in n . In addition, a more noteworthy influence might be seen for $n < 1$ when compared with $n > 1$.

In order to visualize the development of the momentum and thermal boundary layers for Sisko fluid, the velocity and temperature profiles for different values of the magnetic parameter M are plotted in Figs. 3 and 4, respectively. Figure 3 tracks the evolution of the velocity profile for varying values of the power-law index n . It can be observed from this figure that an increment in value of the magnetic parameter M resulted in reduction of the velocity as well as the boundary layer thickness. This is because of the resistance of the drag force produced by the magnetic field. Besides, these figures reveal a correlation that the magnitude of the velocity is larger

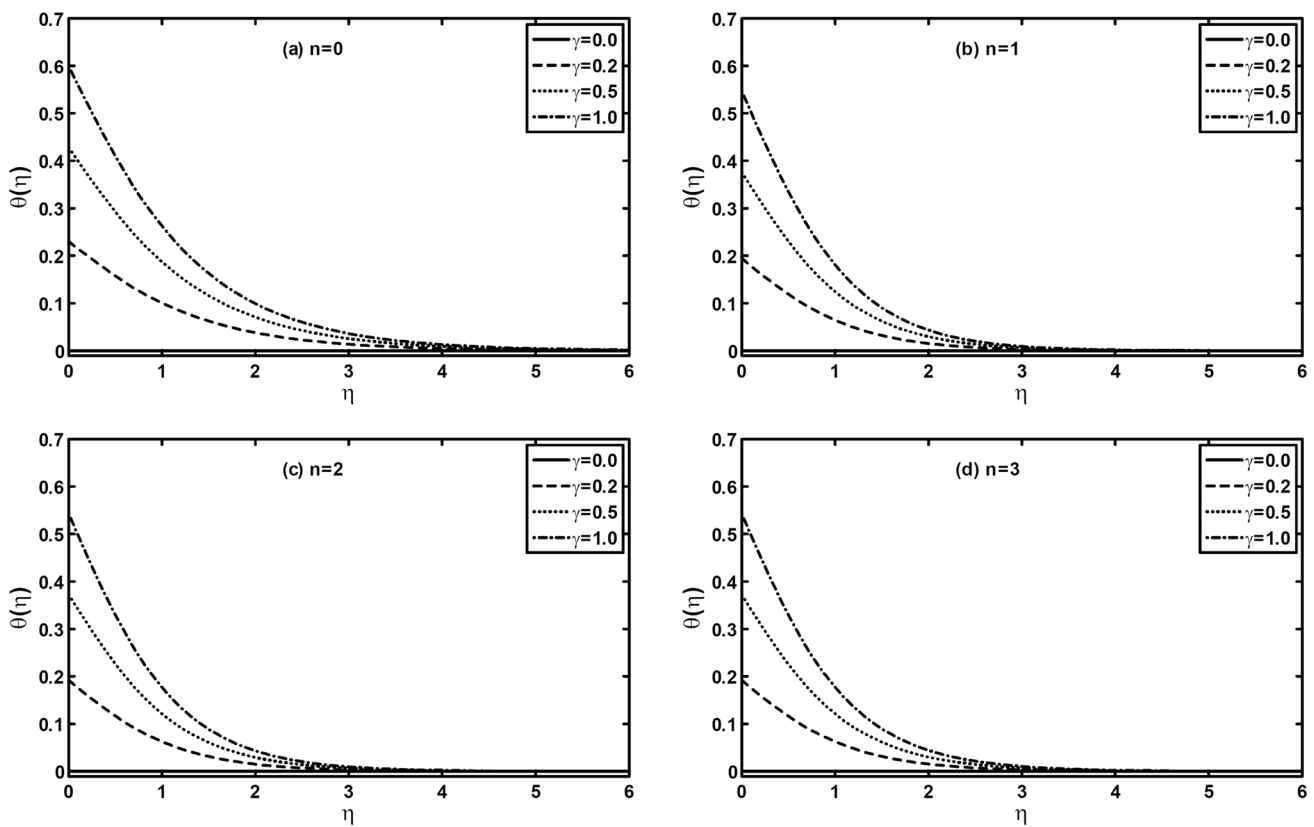


Fig. 6 The temperature profiles $\theta(\eta)$ for different values of the generalized Biot number γ when $A = Pr = M = 1$ and $s = 1/2$ are fixed

for hydrodynamic case ($M = 0$) when contrasted with hydromagnetic case ($M \neq 0$). Figure 4 tracks the evolution of the temperature profile for different values of the magnetic parameter M . It is quite clear from these figures that the effects of the magnetic parameter M on the temperature field and thermal boundary layer are quite opposite to those for velocity. These figures, apart from demonstrating the effects of the magnetic parameter, also show that the influence of the magnetic parameter M gets less overwhelming as we go on increasing the value of the power-law index n .

The effects of the generalized Prandtl number Pr on the temperature profile are shown in Fig. 5. It can be seen that as the generalized Prandtl number increases the temperature profile decreases. This is because of the fact that the fluids with higher Prandtl number possess low thermal conductivity which reduces the conduction and hence the thermal boundary layer thickness.

Figure 6 shows the influence of the generalized Biot number γ on the temperature profile. For $\gamma = 0$, the bottom side of the sheet with the hot fluid is totally insulated and as a result no convective heat transfer to the cold fluid above the sheet takes place. It is observed from the profiles presented in these figures that as the

generalized Biot number γ increases, the temperature profile increases significantly. This further results in an increase in the thermal boundary layer thickness. This is because of the fact that the increase in the Biot number resulting in an increase in convection which reduces the sheet thermal resistance.

The effect of the material parameter A on the temperature field is shown in Fig. 7. This figure also provides a comparison of the temperature profiles of the Sisko fluid ($A \neq 0$) with those of the power-law fluid ($A = 0, n \neq 1$) and the Newtonian fluid ($A = 0, n = 1$). It is seen that as A increases, the temperature profile and corresponding thermal boundary layer thickness decrease for $n = 0, 1, 2$ and 3. Hence, we conclude from these figures that the temperature of Newtonian fluid is higher than that of the Sisko fluid. Further, the temperature for the power-law fluid is also higher than that of the Sisko fluid.

Figures 8 and 9 as well as Tables 2 and 3 show the comparison of temperature field, the local skin-friction coefficient $\frac{1}{2}Re_b^{\frac{1}{n+1}}C_f$ and the local Nusselt number $Re_b^{-\frac{1}{n+1}}Nu$ among the exact, HAM and numerical results. Here it is seen that the comparison is in very

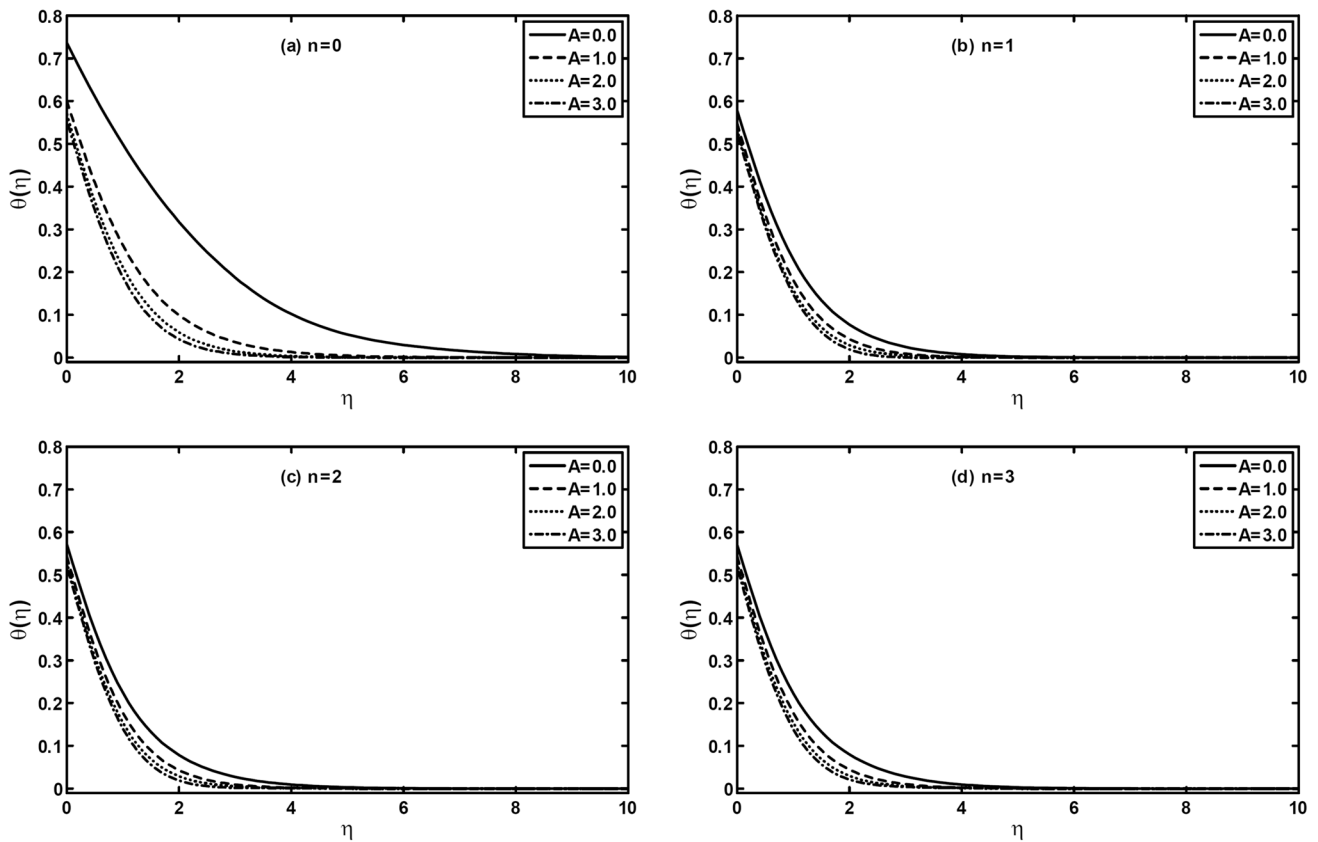


Fig. 7 The temperature profiles $\theta(\eta)$ for different values of the material parameter A when $\gamma = Pr = M = 1$ and $s = 1/2$ are fixed

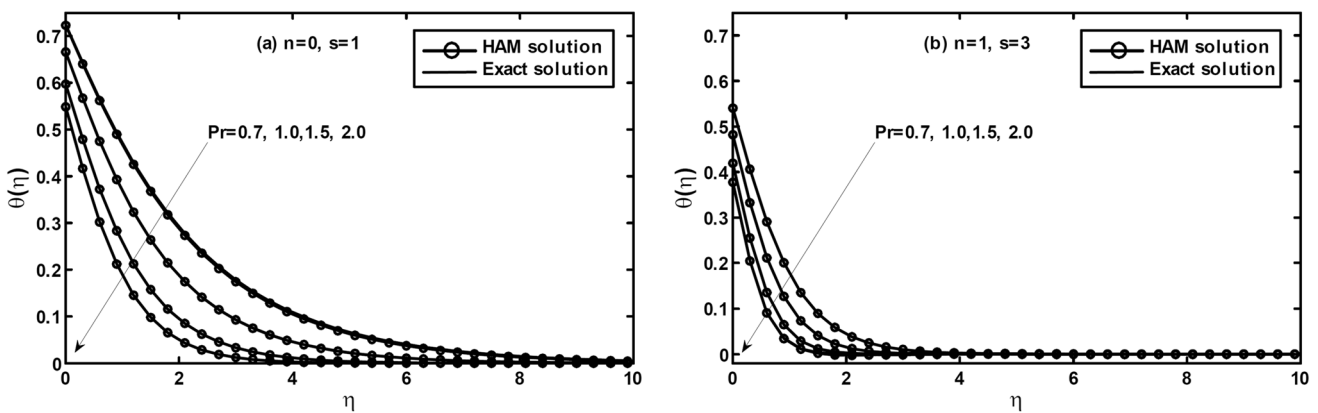


Fig. 8 A comparison of the HAM and exact solutions for the temperature profile $\theta(\eta)$ when $M = A = 1$ and $\gamma = 1$ are fixed

good agreement and thus gives us confidence to the accuracy of the HAM results. Further, the variation of the local skin-friction coefficient and the local Nusselt number is shown in Tables 4 and 5, respectively. These tables show that the magnitude of the local skin-friction coefficient and local Nusselt number is larger for Sisko fluid

when compared to the power-law fluid as well as Newtonian fluid. Additionally, by comparing the hydrodynamic case with hydromagnetic case we can see that the magnitude of the local skin-friction coefficient is larger in the later case whereas for the local Nusselt number results are opposite qualitatively. Also, it is seen that the local

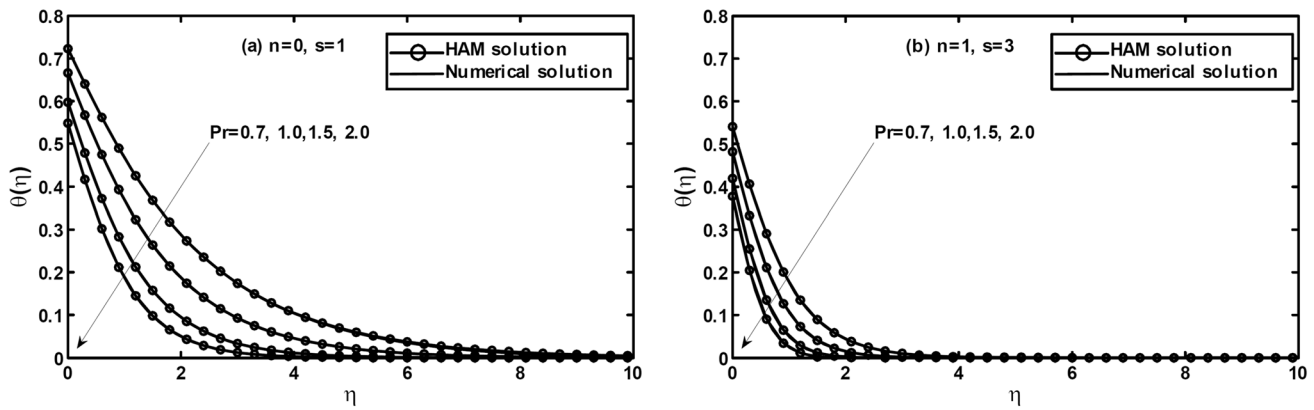


Fig. 9 A comparison of the HAM and numerical solutions for the temperature profile $\theta(\eta)$ when $M = A = 1$ and $\gamma = 1$ are fixed

Table 2 A comparison between the HAM and exact solutions for the skin-friction coefficient

M	A	$-\frac{1}{2} \text{Re}_b^{-\frac{1}{n+1}} C_f$			
		$n = 0, s = 1$		$n = 1, s = 3$	
		Exact solution	HAM solution	Exact solution	HAM solution
1.0	0.0	1.000000	1.000000	2.000000	2.000000
1.0	0.5	2.000000	2.000000	2.449489	2.449489
1.0	1.0	2.414213	2.414213	2.828427	2.828427
1.0	1.5	2.732050	2.732050	3.162277	3.162277
1.0	2.0	3.000000	3.000000	3.464101	3.464101
2.0	0.0	1.000000	1.000000	2.645751	2.645751
2.0	0.5	2.581138	2.581138	3.240370	3.240370
2.0	1.0	3.236067	3.236067	3.741657	3.741657
2.0	1.5	3.738612	3.738612	4.183300	4.183300
2.0	2.0	4.162277	4.162277	4.582575	4.582575

skin-friction coefficient is an increasing function of A , M and s while it decreases with the increasing values of the power-law index n . Additionally, the local Nusselt

number shows an increasing behavior for A , Pr , γ and s while decreasing behavior for M .

6 Conclusions

This study has dealt with the analysis of an MHD flow and convective heat transfer of the Sisko fluid considering the convective boundary conditions at the wall over a nonlinearly radially stretching sheet. The analytical and numerical solutions for the velocity and temperature fields were constructed by using the HAM and shooting method, respectively. The obtained analyzed solutions were compared in a very good agreement with the exact solutions.

The main contributions of our work were the analytical results for the velocity and temperature fields for an electrically conducting Sisko fluid. From the analysis of our results, one may conclude that inside the boundary layer the value of n affected significantly the velocity field but marginally the temperature field. Our illustrative results have showed that the effects of the magnetic parameter on

Table 3 A comparison between the HAM and exact solutions for the local Nusselt number

A	M	Pr	γ	$-\text{Re}_b^{-\frac{1}{n+1}} Nu$			
				$n = 0, s = 1$		$n = 1, s = 3$	
				Exact solution	HAM solution	Exact solution	HAM solution
1.0	1.0	1.0	0.1	0.083367	0.083367	0.091490	0.091490
1.0	1.0	1.0	0.2	0.142959	0.142959	0.168632	0.168632
1.0	1.0	1.0	0.5	0.250312	0.250312	0.341291	0.341291
1.0	1.0	1.0	1.0	0.333888	0.333888	0.518121	0.518121
1.0	1.0	2.0	0.1	0.089166	0.089166	0.094278	0.094278
1.0	1.0	2.0	0.2	0.160900	0.160900	0.178353	0.178353
1.0	1.0	2.0	0.5	0.311041	0.311041	0.383607	0.383607
1.0	1.0	2.0	1.0	0.451465	0.451465	0.622343	0.622343

Table 4 Numerical values of the skin-friction coefficient $\frac{1}{2} \text{Re}_b^{-\frac{1}{n+1}} C_f$ for different values of physical parameters

A	M	s	$-\frac{1}{2} \text{Re}_b^{-\frac{1}{n+1}} C_f$			
			n = 0	n = 1	n = 2	n = 3
0.0	1.0	0.5	1.000000	1.395883	1.369854	1.357321
1.0			2.362506	1.974077	1.852944	1.790524
2.0			2.926875	2.417741	2.273963	2.203414
1.0	0.0	0.5	1.939180	1.399534	1.280257	1.220124
	1.0		2.362506	1.974077	1.852944	1.790524
	2.0		3.200468	3.139790	3.145211	3.149431
1.0	1.0	0.5	2.362506	1.974077	1.852944	1.790524
		1.0	2.414214	2.171823	2.117189	2.092716
		2.0	2.527525	2.521496	2.590447	2.645556

Table 5 Numerical values of the local Nusselt number $\text{Re}_b^{-\frac{1}{n+1}} Nu$ for different values of physical parameters

A	M	Pr	γ	s	$-\text{Re}_b^{-\frac{1}{n+1}} Nu$			
					n = 0	n = 1	n = 2	n = 3
0.0	1.0	1.0	1.0	0.5	0.252262	0.422551	0.428277	0.429523
1.0					0.399606	0.452675	0.456642	0.457250
2.0					0.430592	0.465420	0.469661	0.470823
1.0	0.0	1.0	1.0	0.5	0.427702	0.470063	0.471092	0.470521
	0.5				0.419895	0.465321	0.467117	0.466791
	1.0				0.399606	0.452675	0.456642	0.457250
1.0	1.0	0.7	1.0	0.5	0.338044	0.395301	0.397475	0.397133
		1.0			0.399606	0.452675	0.456642	0.457250
		2.0			0.516778	0.559069	0.564852	0.566769
1.0	1.0	1.0	0.1	0.5	0.086938	0.089213	0.089366	0.089390
			0.5		0.285513	0.311615	0.313489	0.313776
			1.0		0.399606	0.452675	0.456642	0.457250
1.0	1.0	1.0	1.0	0.5	0.399606	0.452675	0.456642	0.457250
				1.0	0.333889	0.468686	0.489573	0.498138
				2.0	0.028896	0.495793	0.537845	0.554844

the velocity and temperature fields were quite opposite. Our results further revealed that the temperature was increased significantly with an increase in the convective heat transfer parameter. Additionally, it was noted that the temperature of the Sisko fluid was smaller than those of the power-law and Newtonian fluids.

References

- Na TY, Hansen AG (1967) Radial flow of viscous non-Newtonian fluids between disks. *Int J Nonlinear Mech* 2:261–273
- Khan M, Shahzad A (2013) On boundary layer flow of a Sisko fluid over a stretching sheet. *Quaest Math* 36:137–151
- Siddiqui AM (2013) Analytic solution for the drainage of Sisko fluid film down a vertical belt. *Appl Appl Math* 8:465–480
- Khan M, Shahzad A (2012) On axisymmetric flow of Sisko fluid over a radially stretching sheet. *Int J Nonlinear Mech* 47:999–1007
- Hayat T, Iqbal Z, Mustafa M, Alsaedi A (2012) Momentum and heat transfer of an upper-convected Maxwell fluid over a moving surface with convective boundary conditions. *Nucl Eng Des* 252:242–247
- Makinde OD, Chinyoka T, Rundora L (2011) Unsteady flow of a reactive variable viscosity non-Newtonian fluid through a porous saturated medium with asymmetric convective boundary conditions. *Comput Math Appl* 62:3343–3352
- Hayat T, Iqbal Z, Qasim M, Obaidat S (2012) Steady flow of an Eyring Powell fluid over a moving surface with convective boundary conditions. *Int J Heat Mass Transf* 55:1817–1822
- Rundora L, Makinde OD (2013) Effects of suction/injection on unsteady reactive variable viscosity non-Newtonian fluid flow in a channel filled with porous medium and convective boundary conditions. *J Pet Sci Eng* 108:328–335
- Ramesh GK, Gireesha BJ (2014) Influence of heat source/sink on a Maxwell fluid over a stretching surface with convective

- boundary condition in the presence of nanoparticles. *Ain Shams Eng J.* doi:[10.1016/j.asej.2014.04.003](https://doi.org/10.1016/j.asej.2014.04.003)
10. Shehzad SA, Alsaedi A, Hayat T (2012) Three-dimensional flow of Jeffrey fluid with convective surface boundary conditions. *Int J Heat Mass Transf* 55:3971–3976
 11. Nadeem S, Mehmood R, Akbar NS (2014) Optimized analytical solution for oblique flow of a Casson-nano fluid with convective boundary conditions. *Int J Therm Sci* 78:90–100
 12. Hayat T, Shafiq A, Alsaedi A (2014) Effect of joule heating and thermal radiation in flow of third grade fluid over radiative surface. *PLoS One* 9(1):e83153. doi:[10.1371/journal.pone.0083153](https://doi.org/10.1371/journal.pone.0083153)
 13. Hayat T, Shafiq A, Alsaedi A, Awais M (2013) MHD axisymmetric flow of third grade fluid between stretching sheets with heat transfer. *Comput Fluids* 86:103–108
 14. Khan WA, Khan M, Malik R (2014) Three-dimensional flow of an Oldroyd-B nanofluid towards stretching surface with heat generation/absorption. *PLoS One* 9(8):e105107. doi:[10.1371/journal.pone.0105107](https://doi.org/10.1371/journal.pone.0105107)
 15. Liao S (2012) *Homotopy analysis method in nonlinear differential equations*. Springer, London